Urban Climate 64 (2025) 102664

Contents lists available at ScienceDirect

Urban Climate

journal homepage: www.elsevier.com/locate/uclim

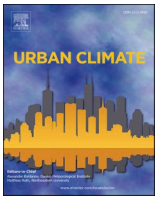

A fast and automated approach for urban CFD simulations: validation with meteorological predictions and its application to drone flights

Marcos Suárez-Vázquez [a,b,c], Sylvana Varela Ballesta [a,d], Alberto Otero-Cacho [b,c], Alberto P. Muñuzuri [b,c], Jorge Mira [e,*]

[a] Ventilatio Lab S.L., 15782 Santiago de Compostela, Spain
[b] Galician Center for Mathematical Research and Technology (CITMAga), 15782 Santiago de Compostela, Spain
[c] Group of Nonlinear Physics, Universidade de Santiago de Compostela, 15782 Santiago de Compostela, Spain
[d] Departament d'Enginyeria Mecànica, University Rovira i Virgili, 43007 Tarragona, Spain
[e] Departamento de Física Aplicada and Instituto de Materiais (iMATUS), Universidade de Santiago de Compostela, 15782 Santiago de Compostela, Spain

ARTICLE INFO

Keywords:
Computational fluid dynamics
Urban planning
Terrain reconstruction
Building reconstruction
Validation study
Drones
Wind tunnel

ABSTRACT

In past years, several studies have proposed new methods and applications for urban wind simulations, including geometry reconstruction from urban data sources or improved boundary condition definition. In this article, we present a fast and automated methodology for reconstructing airflows within urban environments using LiDAR and cadastral data coupled with Computational Fluid Dynamics (CFD) simulations. Our approach integrates meteorological predictions with computational techniques to simulate the complex interactions between wind currents, buildings, vegetation, water zones and terrain morphology within urban environments. Accurate boundary conditions based on meteorological predictions are introduced into a coupled methodology that directly creates the terrain shape inside the simulation environment, simplifying the geometry creation process, which is one of the most prevalent problems in CFD urban simulations. The simulation results are confronted against ground-truth real data obtained from a meteorological station, showing strong agreement with the outcomes generated by the proposed CFD model, with a concordance correlation coefficient up to $\rho_c = 0.985$ for the wind direction and $\rho_c = 0.853$ for the wind speed. The results from these simulations are then used for validating a wind tunnel approach that mimics the interaction between a moving drone and the extracted wind currents, demonstrating a great improvement in computation times when compared to the most straightforward approach that consists in embedding the drone within the full urban landscape. This research contributes to the advancement of urban CFD modeling, and it has significant implications for various applications, providing valuable insights for urban development.

* Corresponding author.
E-mail address: jorge.mira@usc.es (J. Mira).

https://doi.org/10.1016/j.uclim.2025.102664
Received 14 July 2025; Received in revised form 26 September 2025; Accepted 17 October 2025
Available online 23 October 2025

1. Introduction

Urban environments are characterized by complex aerodynamic challenges due to the intricate interactions between buildings, orography, vegetation, and atmospheric conditions (Liu et al., 2018; Sandu et al., 2019). The rapid urbanization of densely populated regions across the globe has witnessed a significant growth in recent years (Angel et al., 2005; Bocquier, 2005; Toparlar et al., 2017). Cities, as hubs of economic, social, and cultural activity, have grown exponentially. However, this surge in urbanization has also led to some challenges associated with large population concentrations. Urban climate is recognized as one of the main concerns of the next decade (Mirzaei, 2021), and some widely investigated topics include pollution dispersion in streets (Chu et al., 2005; Fernández-Pacheco et al., 2023), energy demand of buildings (Allegrini et al., 2015), indoor/outdoor air quality (Muñuzuri et al., 2022; Yang et al., 2014), urban design optimization (Valger and Fedorova, 2019) or pedestrian comfort (Antoniou et al., 2019; Blocken et al., 2012).

In the context of urban settings, Unmanned Aerial Vehicles (UAVs), commonly referred to as drones, have also seen a significant increase in use within large cities. The rapid expansion of the drone market (de Miguel Molina and Segarra Oña, 2018) has placed them at the forefront of various applications, including blood transportation (Amukele et al., 2017), delivery of sensitive medical equipment (Haidari et al., 2016; Pulver et al., 2016), or animal tracking and detection (Chabot and Francis, 2016; Koger et al., 2023). Drones also play a crucial role in disaster management, assisting in flood and earthquake response efforts (Mishra et al., 2020; Restas, 2015), as well as in media broadcasting (Ayranci, 2016). Additionally, they have revolutionized package shipping and distribution (Benarbia and Kyamakya, 2021), significantly reducing costs, delivery times, and emissions compared to traditional alternatives (Rajabi et al., 2023).

The modeling of wind patterns within urban environments has become an incredibly helpful asset to improving most of these applications. Computational Fluid Dynamics (CFD) simulations have emerged as a powerful tool for simulating airflow within urban areas, offering non-invasive insights into the generated airflow patterns, both for past experiments and future predictions. In the last years, a great number of building reconstruction tools (e.g., Dhunny et al., 2018; Liu et al., 2017; Toparlar et al., 2018) have been proposed, even though they are not always adapted for CFD simulations. Some of them include flat terrains surrounding the buildings, which is a great disadvantage as demonstrated in (Brozovsky et al., 2021), where the introduction of real terrain morphology is needed.

In (Paden et al., 2022; Paden et al., 2024), the authors propose a very useful method for the reconstruction of urban environments using LiDAR and cadastral data. However, this approach lacks the automation capabilities to be used for real-time predictions, as its use is restricted to geometry generation, and lacks the implementation of automatic and complete simulations with accurate boundary conditions that correctly transmit low-resolution meteorological predictions into detailed simulations. Furthermore, challenges still persist in validating such models against real-world data, as highlighted in Ju et al. (2021), who note that over 50% of urban microclimate studies lack rigorous validation.

In recent years, some reference guidelines have been published for many aspects of urban simulations (e.g., Blocken, 2015). Concepts such as the area of interest, which defines the optimal number of building blocks relative to a building of interest to achieve accurate simulations, and outer domain boundary sizes, are treated. Other aspects, such as the mesh type and its convergence study, the boundary conditions or the roughness parameter modeling have also been extensively studied, making urban CFD simulations more and more precise. However, these types of simulations are usually still very computationally expensive, needing large amounts of time for the generation and execution of precise simulations valid for real life applications as the ones previously mentioned.

In this article, we embark on a comprehensive study employing CFD simulations to analyze urban airflow dynamics, with a particular focus on leveraging meteorological predictions and observational data from real-life meteorological stations. The geometry generation is facilitated by the use of an algorithm that combines cadastral data and point cloud LiDAR technology, commonly used for reconstructing urban geometries (Alonso and Malpica, 2010). Accurate boundary conditions are generated from meteorological predictions, and the influence of vegetation and water zones is incorporated into the airflow patterns of our simulations. This process is completely automated and can be applied to virtually any region in the world, with low execution times that allow its usage for applications where low response times are crucial. To account for an application of this methodology and further optimize computation times, the extracted wind field data from the urban simulation is used in an independent virtual wind tunnel simulation. This approach calculates aerodynamic parameters and load magnitudes over a drone geometry inside a small wind tunnel, which are then compared with the results from a direct, time-consuming simulation performed directly over a moving drone within the entire city reconstruction. The results from both simulations are compared, and the improvement in computational cost is analyzed.

The primary aim of this research is to validate the accuracy of the proposed urban reconstructions and CFD simulations against observational data from meteorological stations, thereby enhancing confidence in computational predictions of urban airflow and assessing them in real-life scenarios, like a moving drone in a pre-planned path, where fast and accurate responses are needed under varying conditions. The predictions obtained by this method can be used for providing a better understanding of the airflow patterns that emerge in urban environments. This understanding can have a great utility for a wide range of applications, such as assessing the viability of UAV flights under certain meteorological conditions. Other potential applications of this reconstruction methodology include the optimization of ventilation in enclosed spaces by analyzing wind fields around buildings, as well as the study of sound dispersion and acoustics in open areas, which are heavily influenced by obstacles and fluctuating air currents. Additional applications include the analysis of pollution dispersion by the incorporation of traffic models or the study of fire propagation.

This paper is structured as follows. First, we present the geometry reconstruction methodology and describe the virtual wind tunnel developed for the drone. Next, we compare the simulated wind field with real-world data recorded at a meteorological station. Finally, we evaluate the wind tunnel approach using a generic drone geometry and compare its results with those obtained from a more computationally intensive simulation of the drone moving through an urban environment.

2. Methodology

2.1. Numerical simulations using CFD techniques

Numerical simulations were conducted to analyze air circulation within the computational domain. The commercial software Simcenter STAR-CCM+ (Siemens Digital Industries Software, 2021) was used to design the domain, build the polyhedral meshes, solve the governing conservation equations (Navier-Stokes) using Finite Volume Methods (FVM) (Ferziger et al., 2019) and post-process the results. The equations for the conservation of mass and momentum (Kundu et al., 2024) read as in Eqs. (1) and (2),

$$\frac{\partial}{\partial t}\int_V \rho dV + \oint_A \rho \boldsymbol{v}\cdot\boldsymbol{n}\, dA = \int_V S_m dV, \# \tag{1}$$

$$\frac{\partial}{\partial t}\int_V \rho \boldsymbol{v}\, dV + \oint_A (\rho \boldsymbol{v}\otimes\boldsymbol{v})\cdot\boldsymbol{n}\, dA = -\oint_A p\boldsymbol{n}\cdot dA + \oint_A \boldsymbol{T}\cdot\boldsymbol{n}\, dA + \int_V \boldsymbol{f_b}\, dV + \int_V S_u dV, \# \tag{2}$$

where t is time, V is the control volume, A is the control surface with outward unit normal $\mathbf{n}$, ρ is the density, $\boldsymbol{v}$ is the velocity vector, p is the pressure, $\boldsymbol{T}$ is the viscous stress tensor, $\boldsymbol{f_b}$ is the body force per unit volume, S_m is the mass source term, and S_u is the user-specified source term.

An incompressible solver with constant density was selected, along with a realizable k-ε turbulent Reynolds-Averaged Navier-Stokes (RANS) model, considered suitable for numerical simulations of urban environments (Parente et al., 2011a; Wang and McNamara, 2006). In addition, an enhanced wall treatment with a two layer approach (Rodi, 1991) was used to gain flexibility of an all $-y^+$ wall treatment. SIMPLE algorithm was used for pressure-velocity coupling and a second-order upwind discretization scheme was chosen for the conservation of mass and momentum equations.

The transport equations for the kinetic energy k and the turbulent dissipation rate ε of the turbulence model are given as in Eqs. (3) and (4),

$$\frac{\partial}{\partial t}(\rho k) + \nabla\cdot(\rho k\overline{\boldsymbol{v}}) = \nabla\cdot\left[\left(\mu + \frac{\mu_t}{\sigma_k}\right)\nabla k\right] + P_k - \rho(\varepsilon - \varepsilon_0) + S_k, \# \tag{3}$$

$$\frac{\partial}{\partial t}(\rho \varepsilon) + \nabla\cdot(\rho \varepsilon\overline{\boldsymbol{v}}) = \nabla\cdot\left[\left(\mu + \frac{\mu_t}{\sigma_\varepsilon}\right)\nabla \varepsilon\right] + \frac{1}{T_\varepsilon}C_{\varepsilon 1}P_\varepsilon - C_{\varepsilon 2}f_2\rho\left(\frac{\varepsilon}{T_\varepsilon} - \frac{\varepsilon_0}{T_0}\right) + S_\varepsilon, \# \tag{4}$$

where $\overline{\boldsymbol{v}}$ is the mean velocity; μ is the dynamic viscosity; $\sigma_k = 1.0$, $\sigma_\varepsilon = 1.2$, $C_{\varepsilon 1} = 1.44$, and $C_{\varepsilon 2} = 1.9$ are the model coefficients; f_2 is a damping function; S_k and S_ε are the user-specified source terms, and P_k and P_ε are the production terms defined by Eqs. (5) and (6),

$$P_k = f_c G_k + G_b - \gamma_M, \# \tag{5}$$

$$P_\varepsilon = f_c S_k + C_{\varepsilon 3} G_b, \# \tag{6}$$

where $C_{\varepsilon 3} = tanh(|v_b|/|u_b|)$ is a model coefficient in which u_b and v_b are the velocity components parallel and perpendicular to the gravitational vector $\boldsymbol{g}$, f_c is the curvature correction factor, G_b and G_k are buoyancy and turbulent production, $\gamma_M$is the compressibility modification, $f_2 = k/(k + \sqrt{\nu\varepsilon})$ is a damping function and $S_{k,\varepsilon}$ are the user-defined source terms, which are not explicitly used in our simulations.

2.2. Geometry reconstruction

In order to perform the CFD simulations, in which both the terrain orography and the presence of buildings play a crucial role, we first need to generate an appropriate geometry (manifold and watertight), so that the CFD software can process it effectively. To achieve this, we developed an algorithm capable of reconstructing geometries using information from two distinct datasets: LiDAR point cloud height data and cadastral information defining building footprints.

Fortunately, Spain provides well-documented and easily accessible LiDAR datasets that contain height information for every point (0.5–14 points/m^2), classified into various labels such as ground, vegetation, water, and buildings. This data, filtered using a Python script, provides a good notion of not only the height of a specific point, but also the buildings density in the desired area. Cadastral data is the other necessary dataset, as it helps to define building footprints for the generation of precise geometries. For the case of Spain, it can be accessed and downloaded using a QGIS plug-in (Shurupov et al., 2023), which provides a simple tool for downloading the information in an appropriate format.

The first step in our approach is the terrain reconstruction, from which the building geometries are then generated. A significant advantage of our all-in-one methodology is the direct integration between the Python code and the CFD simulations. By linking the code with Java macros inside Star-CCM+, we do not need to export the geometry before importing it into the software. This approach is particularly beneficial, as one of the main challenges in urban CFD simulations consists in preparing watertight and manifold geometry. Directly exporting the terrain would not only increase computational time but also introduce geometry errors that could require manual correction.

Instead of this, we generate a file that contains the height information of every terrain point within the domain. This file serves as a

reference velocity for a Morphing motion inside the simulation, which deforms the domain to mimic the real terrain shape. As a result, real-life terrain features can be replicated by morphing the geometry directly inside the simulation software. Additionally, an .stl file with the shape of the ground is also generated for post-processing purposes, as it helps visualize velocity fields at a given height over the ground.

The 3D modeling of the buildings is constructed using a Level of Detail (LoD) of 1.2 according to the classification in (Biljecki et al., 2016). This means that the buildings are reconstructed using the shape given by the cadastral dataset and raised to a uniform height equal to the mean height of the LiDAR points that fall into the building footprints. This level of detail corresponds to the approximated model in (Ricci et al., 2017), which maintains a good fidelity in terms of wind flows in comparison to a more detailed model. It should be stressed that higher LoD values than the one considered are not only significantly more complex to reconstruct—requiring much more accurate data—but would also considerably slow down the simulations. Fig. 1 shows the geometry used for calibrating our methodology.

As we are working with a LoD 1.2 (i.e., buildings with flat roofs), in which the vertices of the top and bottom surfaces only differ in their z coordinate, the greatest complexity for generating the geometry resides in triangulating the base of the building. For doing that, we chose to use the Ear Clipping algorithm (Eberly, 2008), which is a method for triangulating a non-self-intersecting polygon. It works by iteratively identifying and removing ears—triangular sub-regions that can be clipped from the polygon without affecting its overall shape.

An ear is defined as a triangle formed by three consecutive vertices (v_i, v_{i+1}, v_{i+2}) of the polygon, where v_{i+1} (the middle vertex) is convex, and the triangle does not contain any other vertices of the polygon inside it. The algorithm proceeds as follows:

1. It starts with a simple polygon, represented as an ordered list of vertices. It identifies the convex vertices of the polygon, which are potential ear candidates.
2. An ear is defined as a triangle formed by three consecutive vertices (v_i, v_{i+1}, v_{i+2}) of the polygon, where v_{i+1} is convex (i.e., its internal angle is less than 180°) and the triangle does not contain any other vertices of the polygon inside it. The algorithm scans through the polygon to detect all valid ears.
3. A detected ear is removed from the polygon by eliminating its middle vertex v_{i+1}. The remaining polygon is updated, and the process continues with the next available ear.
4. Once an ear is clipped, the polygon shrinks. The new neighboring vertices are checked to see if they form new ears, and the process adapts to the updated shape of the polygon.
5. Steps 2–4 are repeated until only one triangle remains in the polygon. The final result is a triangulated polygon, where all the interior regions are covered by non-overlapping triangles.

This triangulation for the building's bottom surface is then copied for the top face, and the lateral faces are easily calculated. This process is iterated for every building inside the domain, and the geometry is finally exported, as seen in Fig. 1(c). It is important to note that this process of geometry generation is completely automated, as we only have to provide the coordinates of the region we want to reconstruct. This makes the entire process extremely fast, and once this information is provided, the whole process is automatic.

Even though the area of interest and outer domain sizes are completely customizable inside the configuration file, the dimensions

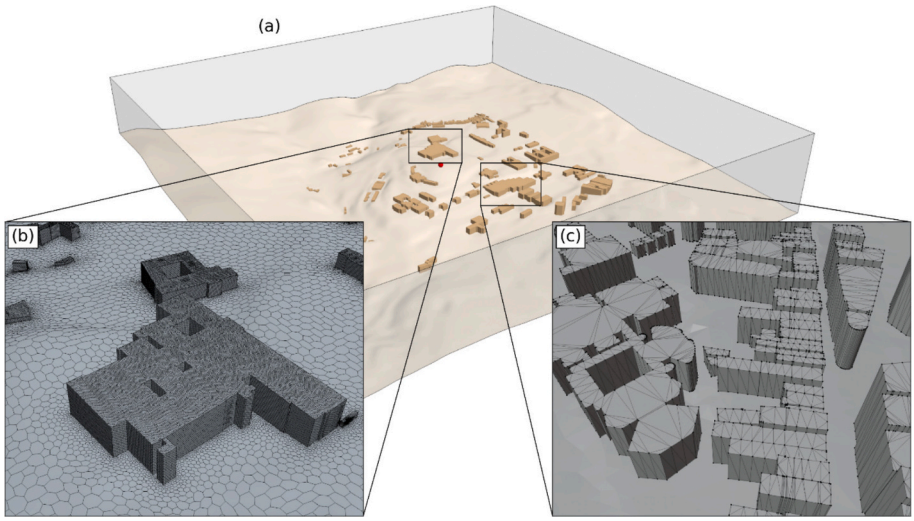

Fig. 1. (a) Geometry used for the calibration process representing the Campus Sur in the University of Santiago de Compostela (Spain). The red dot represents the meteorological station from the official Galician weather service (MeteoGalicia), which we will use as a ground-truth reference value to assess the validity of our methodology. (b) Mesh used for the simulations. (c) Example of the resulting triangulation extracted from the Ear Clipping algorithm. (For interpretation of the references to colour in this figure legend, the reader is referred to the web version of this article.)

are set in a way that meet the directional blockage ratios proposed in (Blocken, 2015). This type of reference values is usually assigned to simple simulations with flat terrain

and aligned buildings, but in real environments the analysis becomes a little harder. In our case, we select the tallest building—not the one situated in the highest part—and choose the minimum domain height (i.e., the distance between the highest point of the ground and the top surface) to reach a minimum blockage height ratio of 17 %, as recommended in (Blocken, 2015). A similar rule is applied for the rest of horizontal ratios.

The number of necessary building layers around the point we want to study, usually called area of interest, is a topic discussed in (Liu et al., 2018). Again, as we are considering real-life morphologies, applying these reference values becomes harder, as we are sometimes not interested in a small area, but rather in a big area or a long path through various streets. For that reason, the area of interest can be modified freely inside the code through a configuration file, but some layers around the area of interest are always needed in order to get precise results in our paths.

Following this discussion, the reconstructed domain used for calibrating the model can be seen in Fig. 1. More examples of geometry reconstructions from different regions in Spain are provided in the Supplementary Material (Figures S.1, S.2 and S.3). In recent years, more countries have started performing LiDAR-based measurements of their territory and others have plans to do so, which means this method could be extended to reconstruct virtually any part of the world once the appropriate datasets are publicly available.

A mesh independence test was performed for this specific geometry. A polyhedral mesh with refinement near the buildings was applied. We assessed five different base sizes in order to search for the best results with the lower number of elements for the mesh in Fig. 1(b). The most meaningful data for each simulation can be found in the Supplementary Material, where different magnitudes are compared in all meshes.

The Wall y+ values are high for the standard of typical CFD simulations, but still in range given the scales with which we are working. Some authors suggest values lower than 1,000 for the majority of the cells, while others extend it to around 10,000 (Aliabadi et al., 2018; Blocken et al., 2007; Li et al., 2019). In our mesh, more than 50% of cells have y+ values below 1,000, while up to 99.5% of them are below 10,000. A more refined mesh near the buildings was considered in order to see if y^+ values should have been optimized, but the wind speed and direction showed less than 1% change, with 7 times the number of cells and the consequent computational cost. Therefore, we can conclude that high y^+ values are acceptable when working with these spatial scales.

2.3. Boundary conditions and modeling of vegetation

To generate appropriate boundary conditions, we have to consider not only the wind speed provided by the meteorological service, but also the height at which it is provided. Intuitively, one can think of the progression of the wind speed as a boundary layer generated by the no-slip condition with the ground. To model this behavior, we will use a RANS model with a neutral Atmospheric Boundary Layer (ABL) logarithmic approximation (Parente et al., 2011b). A frequently used functional form for the velocity, turbulent kinetic energy and dissipation rate for neutral stratification conditions is,

$$v(z) = \frac{u_*}{\kappa} \ln\left(\frac{z + z_0}{z_0}\right), \# \tag{7}$$

$$k = \frac{u_*^2}{\sqrt{C_\mu}}, \# \tag{8}$$

$$\varepsilon = \frac{u_*^3}{\kappa(z + z_0)}, \# \tag{9}$$

where u_* is the friction velocity whose value can be estimated by knowing a reference value for a given height, $\kappa = 0.41$ is the von Karman constant, z is the height above the ground level and z_0 is the roughness parameter, whose typical values depend on the type of surface considered (Wieringa, 1992).

The value of the roughness parameter controls the speed at which the velocity raises its value until reaching the condition imposed for u_*, so lower values for z_0 imply faster growing velocities.

This concept of roughness parameter can also be used to represent the presence of vegetation in the floor of the domain. As previously mentioned, the LiDAR data provides a classification of vegetation into low, medium and high categories. By assigning different roughness lengths (z_0) to each coordinate according to this classification, we can incorporate the effects of vegetation into the terrain's roughness function. This approach indirectly models the presence of different vegetation zones and is particularly useful in areas outside the primary region of interest, where the inlet boundary conditions need sufficient distance to fully develop realistic airflow patterns. Different z0z_0z0 values generate distinct velocity profiles, which influence the flow once it reaches areas with buildings.

Some previous studies have addressed the modeling of vegetation and its influence on urban CFD results (Fu et al., 2024). However, directly representing individual plants or trees typically requires high-precision data and is difficult to automate. To overcome this, we adopted an alternative strategy similar to that used by Di Nicola et al. (2022) and Paden et al. (2022), in which a variable roughness wall parameter is applied to simulate vegetation effects in a computationally efficient and automated manner.

As said before, our code also takes the meteorological predictions at 10 m height from three different sources: the official Galician weather services (MeteoGalicia), the official Spanish weather service (AEMET) and OpenMeteo models. Using these predictions, it

generates appropriate boundary conditions following the logarithmic approximation from Eq. (7). This is not a trivial task, as we are not considering flat terrains near the boundaries. We opted for generating the boundary conditions that preserve Eq. (7) at every point. Fig. 2(a) shows an example of one of the boundary conditions generated for the geometry in Fig. 1, along with an example of the roughness wall parameters used for the different labeled regions in Fig. 2(b).

This whole reconstruction process is, as said before, completely automated. Precise CFD simulations can be generated in less than an hour from scratch, just by downloading the necessary datasets and filling in a configuration file where domain boundaries, meteorological predictions and other information are set.

2.4. Wind tunnel for drone path

The most straightforward approach for evaluating a moving drone's behavior within a wind field derived from an urban CFD simulation consists in embedding the drone geometry directly into the domain and simulating its motion through the flow. However, this method is highly inefficient computationally. It demands fine mesh resolution along the drone's entire path, greatly increasing the number of cells and further amplifying the already substantial computational cost of transient simulations.

To address this limitation, we propose an alternative approach that decouples the drone simulation from the full urban CFD model. Specifically, we use the wind velocity field extracted from a preliminary steady-state CFD simulation of the urban environment as input for a separate, transient simulation conducted in a smaller wind tunnel domain.

A key challenge of this approach is the variability of the wind direction, which would require continuous adjustments of the boundary conditions if the drone remained completely static, potentially causing an inlet boundary to behave like an outlet over time and rendering the simulation unstable. This issue can be easily addressed by setting a constant wind inlet direction and rotating the drone accordingly, which produces an analogous outcome. The rotation of the drone can be achieved using the Overset Mesh technique (Siemens Digital Industries, 2024), which allows for the drone rotation without modifying the direction of the inlet boundary conditions.

A drone traveling at a velocity $\boldsymbol{v}_{drone}$ through a wind field $\boldsymbol{v}_{wind}(\boldsymbol{r})$ is dynamically equivalent to a static drone subjected to a wind field equal to $\boldsymbol{v}_{wind}(\boldsymbol{r}) - \boldsymbol{v}_{drone}$, which is the principle that underlies the operation in wind tunnels. From this concept, we can extract the wind field along any given trajectory from the stationary urban simulation and introduce it into the wind tunnel, with a varying wind speed at the inlet. The drone rotates in real time to align with the wind direction, as experienced by the moving coordinate system traveling along the trajectory at velocity $\boldsymbol{v}_{drone}$.

This setup allows us to compare the results from the wind tunnel simulation to those obtained using the more time-consuming method of embedding the drone within the entire urban domain. Here, we detail the configuration of both simulations and present a comparative analysis. If a strong correlation is observed between the results, the proposed wind tunnel approach can serve as an efficient and faster alternative for evaluating wind loads and aerodynamic forces over optimized trajectories.

To demonstrate the flexibility of our urban reconstruction methodology, we employed a different scenario for the drone simulations compared to the one previously presented. For testing purposes, we selected a flat area with long, uninterrupted streets in the Cuatro Caminos district of Madrid, which allows for a straight, turn-free trajectory of sufficient length. This setup provided an ideal test-bed for validating our approach. Once validated, this methodology can be readily applied to virtually any drone path within any urban environment.

The drone simulation across the full urban domain is initialized using results from a previously conducted steady-state CFD simulation, which provides the baseline wind field. Implementing an Overset Mesh requires careful matching between the background

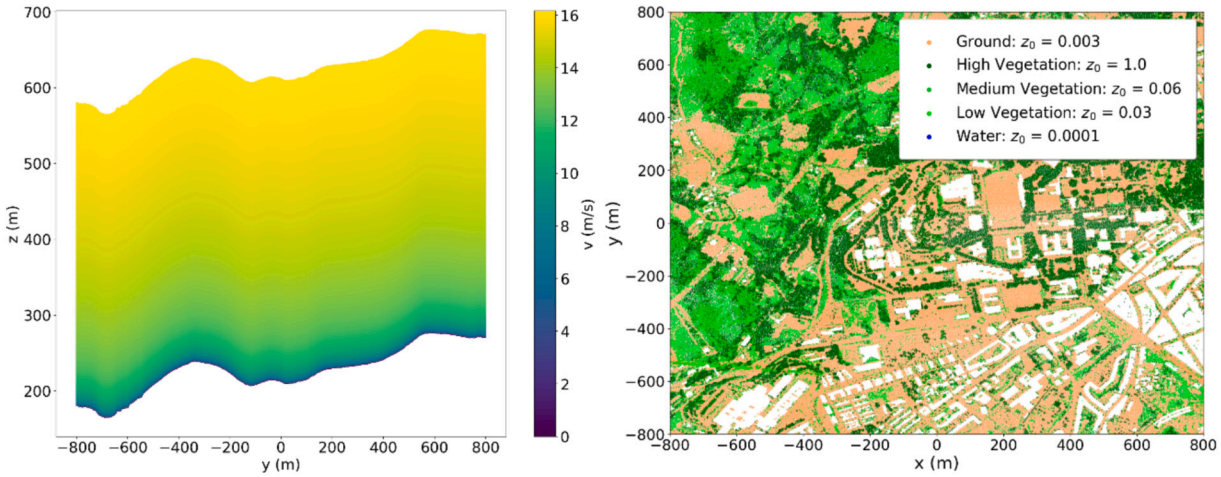

Fig. 2. (a) Example of a boundary condition generated for the calibration geometry in the University of Santiago de Compostela. Note that the ABL equation for velocity is preserved at every point. (b) Vegetation zones inside the domain. The z_0 values are assigned at every point inside the simulation, mimicking the effect of vegetation on the velocity profile.

and overset regions to ensure consistent grid resolution, thereby increasing both the computational cost and setup complexity. An overview of the mesh setup is provided in Fig. 3(a).

For the wind tunnel simulation, a domain with the dimensions and mesh configuration shown in Fig. 3(b) is constructed. The drone geometry, adapted from a generic commercial model and rescaled to match the real size of the DJI Phantom 3 (Paz et al., 2020, 2021), is embedded using the same Overset Mesh technique, with its orientation dynamically updated at each time step to account for changing wind directions. Varying inlet velocities are imposed to emulate the drone's motion through the original urban wind field.

To ensure consistency between the full-domain and wind tunnel simulations, as illustrated in Fig. 3(c,d), a mesh independence study was conducted. We first identified an optimal mesh resolution within the spherical region around the drone in the wind tunnel setup, which was then carried over to the urban reconstruction. Three mesh sizes were tested, with detailed analysis of key reference metrics provided

in the Supplementary Material. Since the drone is enclosed within a spherical Overset Mesh region in both simulations, a consistent mesh size was used throughout. Ensuring comparable donor and acceptor cell sizes necessitates pre-refinement of the drone's path region in the urban domain, significantly increasing cell count and computational load. The background mesh for the broader urban domain is consistent with that used previously for the calibration section, where a dedicated mesh independence assessment was also performed.

3. Results

In this section we will analyze the data extracted from multiple simulations using various meteorological prediction services, comparing the outcomes to real-world observations. Once the accuracy of the methodology is established, we proceed to compare the results from both drone simulations, showing the results compatibility and the difference in computational load.

3.1. Calibration with meteorological station data

The meteorological predictions from the three weather forecast services used in our simulations are provided at different time scales. MeteoGalicia (Weather Research and Forecasting, WRF 1km model) and OpenMeteo provide wind speed and direction at a height of 10 meters every hour for a specific location, whereas AEMET predictions are provided in six-hour intervals with lower resolutions (5 km/h – 45°). While MeteoGalicia and AEMET predictions are uploaded at the start of each day and remain unchanged, OpenMeteo updates its predictions periodically using real-time measurements.

Consequently, downloading the predictions from OpenMeteo for 9:00 AM after that hour has passed will yield corrected predictions, which enables us to use OpenMeteo data as low-resolution ground-truth validation data.

Incorporating these corrected predictions into our model should give closer results to the real data obtained from the meteorological station, while the other two services may provide less accurate results as they are based on future predictions. If the corrected OpenMeteo prediction agrees with the observation data, this means our model is working as expected.

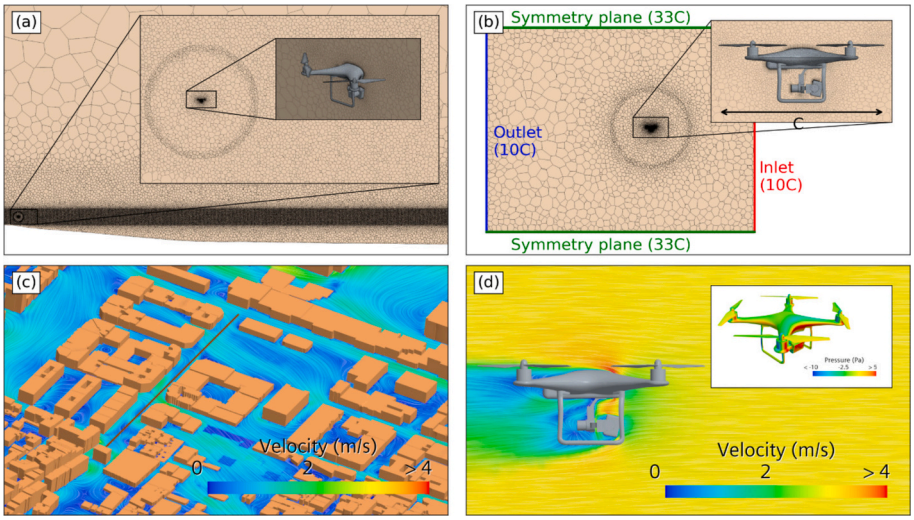

Fig. 3. Overview of the simulation process. We start by selecting an appropriate mesh for both (a) the case of the complete domain over the city reconstruction and (b) the wind tunnel, with the same Base Size for the spherical region around the drone, extracted from a mesh independence test. The dimensions of the tunnel are described relative to the drone's diagonal wingspan $C = 0.4$ m, using the reference values from (Hassan et al., 2014; PrabhakaraRao and Sampath, 2014). Then, (c) the whole city domain is initialized by running a steady simulation, and the wind data is extracted following a given trajectory (brown line). A transient simulation with a moving drone in the whole domain is performed and compared with (d) the wind tunnel approach with lower computational times. (For interpretation of the references to colour in this figure legend, the reader is referred to the web version of this article.)

The meteorological station employed as a reference for validating our simulations is positioned in the center of our wind tunnel (see Fig. 1). This station provides valuable information on wind speed and its direction (along with their corresponding standard deviations) every 10 minutes. Therefore, for every prediction from the MeteoGalicia and OpenMeteo models, the station records up to six measurements of the wind speed. To work with similar time scales in both prediction and observation, and due to the different time discretizations of our predictions, we will use the mean values from 8:30 to 9:30 AM as our real-life measurements, with their corresponding uncertainties.

Inside the simulations, a reference point was positioned at a height of ten meters above ground level at the exact coordinate of the meteorological station. This allowed us to extract wind speed and direction data at that specific point for a direct comparison with the real-life measurements. We can see both the velocity and vorticity fields, which are good indicators for the safety of a given path, for an example simulation in Fig. 4. The average errors for each prediction model are displayed in boxplots in Fig. 5, and a complete comparison for each individual real-life measurement and simulation value is presented in Fig. 6. As evidenced by the boxplots in Fig. 5, OpenMeteo predictions are consistently more accurate than those from the other two services. This was expected, given that OpenMeteo predictions are corrected throughout the day, thereby reproducing sudden changes in meteorological conditions.

A simple way to compare the meteorological station measurements with the simulation results is to plot them together for each prediction service. If the simulations are correct, the points should follow a straight line of slope equal to one and an independent term equal to zero. A linear fit, accounting for the given uncertainties, was performed for each case and is presented in Fig. 7.

The linear fit for the OpenMeteo data is best adjusted to a slope close to one, with an independent term close to zero, both for wind speed and direction. This means that our model for the geometry generation and the creation of boundary conditions for the inlet is working correctly. Consequently, when low resolution data from meteorological predictions is provided, our model can yield accurate local results in terms of the simulated wind speed and direction.

The MeteoGalicia and AEMET predictions are less accurate, as they are not updated in subsequent hours, leaving us with past predictions that have higher error rates. Nevertheless, we observe good predictions for wind direction, whereas wind speed is more challenging to predict due to wind gusts that can affect the results. Despite this, there is a satisfactory agreement for wind speeds in both services, indicated by the positive slopes. The results may be influenced by the lower uncertainties associated with lower wind speed values, which could play a significant role in the linear fits. Both predictions tend to overestimate wind speed, as evidenced by slopes lower than one. This overestimation is preferable since it means we are considering the worst-case scenarios. The spatial and temporal resolution of MeteoGalicia predictions (1 hour) is finer than that of AEMET predictions (6 hours), so the superior results from MeteoGalicia were anticipated.

There are some days in which all three prediction models fail systematically, either in terms of wind speed or direction. However, on other occasions, only OpenMeteo accurately reflects the correct wind components. For instance, on June 21st (see Fig. 6), we could see that the wind direction was very unstable. Examining the registered values from 00:00 AM to 7:00 AM, we observe momentary fluctuations in speed, oscillating around different values. At approximately 9:00 AM, there is a sudden change in direction, and only OpenMeteo successfully reproduces the correct value. In contrast, the other two services indicate completely opposite directions. This discrepancy is largely due to the differing timescales of the predictions; one service predicts this change will occur later, while the other forecasts it earlier.

In the preceding days from July 5th and 6th, the wind consistently registered northeast (NE) component. In those two days, wind direction shifted slightly closer to the north (N), falling between NE and N. This shift resulted in a change in the AEMET prediction, which adjusted from forecasting a direction of 45° (NE) to 0° (N) when this minor change occurred. This adjustment demonstrates the capability of AEMET, as it accurately predicted this small change in wind direction despite its lower resolution in direction and speed. Although AEMET's forecasts are not always precise due to this resolution limitation, it is noteworthy that such a subtle shift was

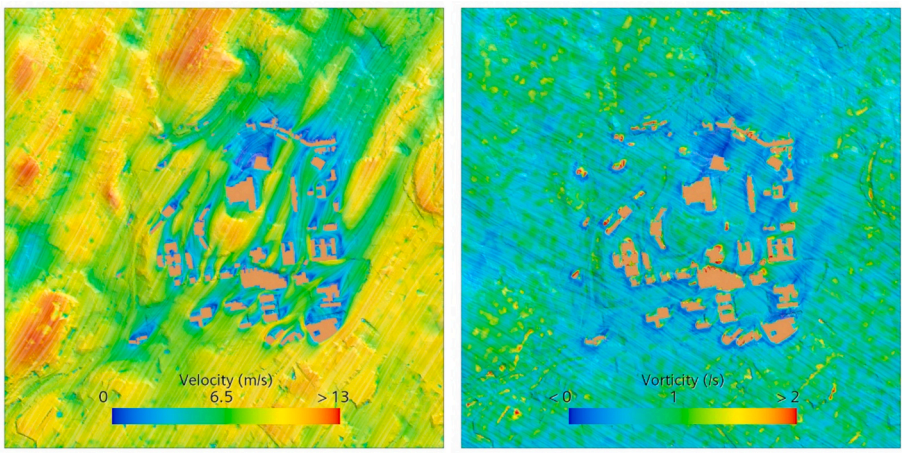

Fig. 4. Visualization of the velocity and vorticity fields in a plane 5 m above ground level for an example simulation in our calibration domain at the Campus Sur of Santiago de Compostela, Spain.

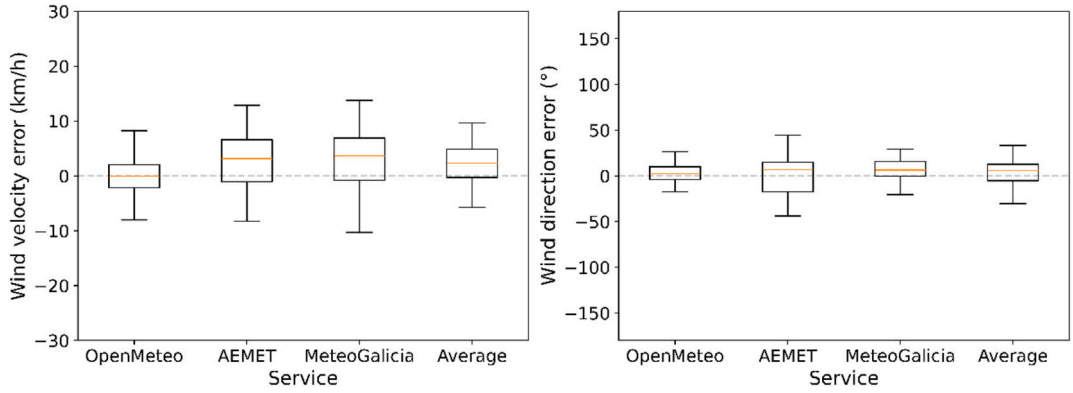

Fig. 5. Boxplot of wind speed and direction errors at 10 m for each model considering the average real-life values over an hour around 9:00 AM.

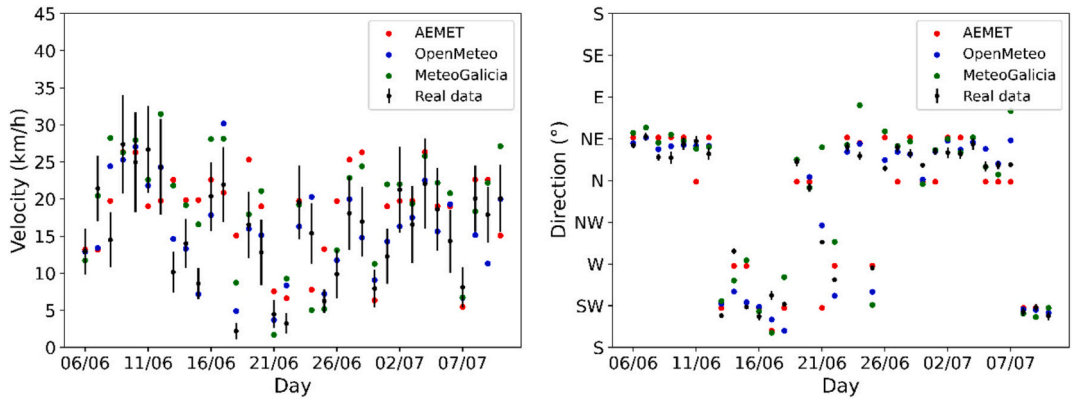

Fig. 6. Comparison of each daily simulation (at 9:00 AM) with its corresponding real-life measurements.

captured, which generally provides the least accurate wind speed predictions.

To quantitatively evaluate the agreement between the simulation results and the real-world measurements, beyond basic linear regression, we employ the Concordance Correlation Coefficient (CCC). Unlike the Pearson correlation coefficient, which only measures the strength of the linear association, the CCC assesses both accuracy (closeness to the identity line) and precision (scatter around the best-fit line). It is therefore ideal for our case, where the goal is to reproduce real-world values as closely as possible using simulated data. The CCC penalizes deviations from both perfect correlation and the ideal 1:1 relationship, making it a comprehensive measure of agreement between predicted and observed wind conditions. The coefficient is defined as,

$$\rho_c = \frac{2\rho\sigma_x\sigma_y}{\sigma_x^2 + \sigma_y^2 + \left(\mu_x - \mu_y\right)^2}, \# \tag{10}$$

where ρ is the Pearson correlation coefficient, μ_x and μ_y are the means of the predicted and observated values, respectively, and σ_x and σ_y are their standard deviations. A CCC value of 1 indicates perfect agreement, while values closer to 0 indicate poorer concordance.

The extracted CCC values of wind speed and direction for each prediction service can be seen in Table 1. Consistently with the previous discussion, we can see an exceptionally good agreement for the OpenMeteo service, while MeteoGalicia and AEMET behave worse given the future-like predictions. Even though the linear fit for direction gives a slope closer to one in the case of MeteoGalicia, the CCC value for OpenMeteo is closer to 1.

3.2. Wind tunnel for a moving drone inside the city

In Section 2.4, we explained the problematic when trying to find the behavior of a moving drone embedding it inside the whole reconstructed domain. The mesh used for the stationary simulations had to be refined all along the drone trajectory in a now transient simulation with constant boundary conditions. To overcome this limitation, we proposed extracting the values from a fast stationary simulation of the city and then using them inside a wind tunnel with a rotating drone and varying inlet velocities replicating the wind currents that the drone encounters while traveling.

The computational time gain is, by far, the greatest reason to use this approach. The execution of the stationary city reconstruction

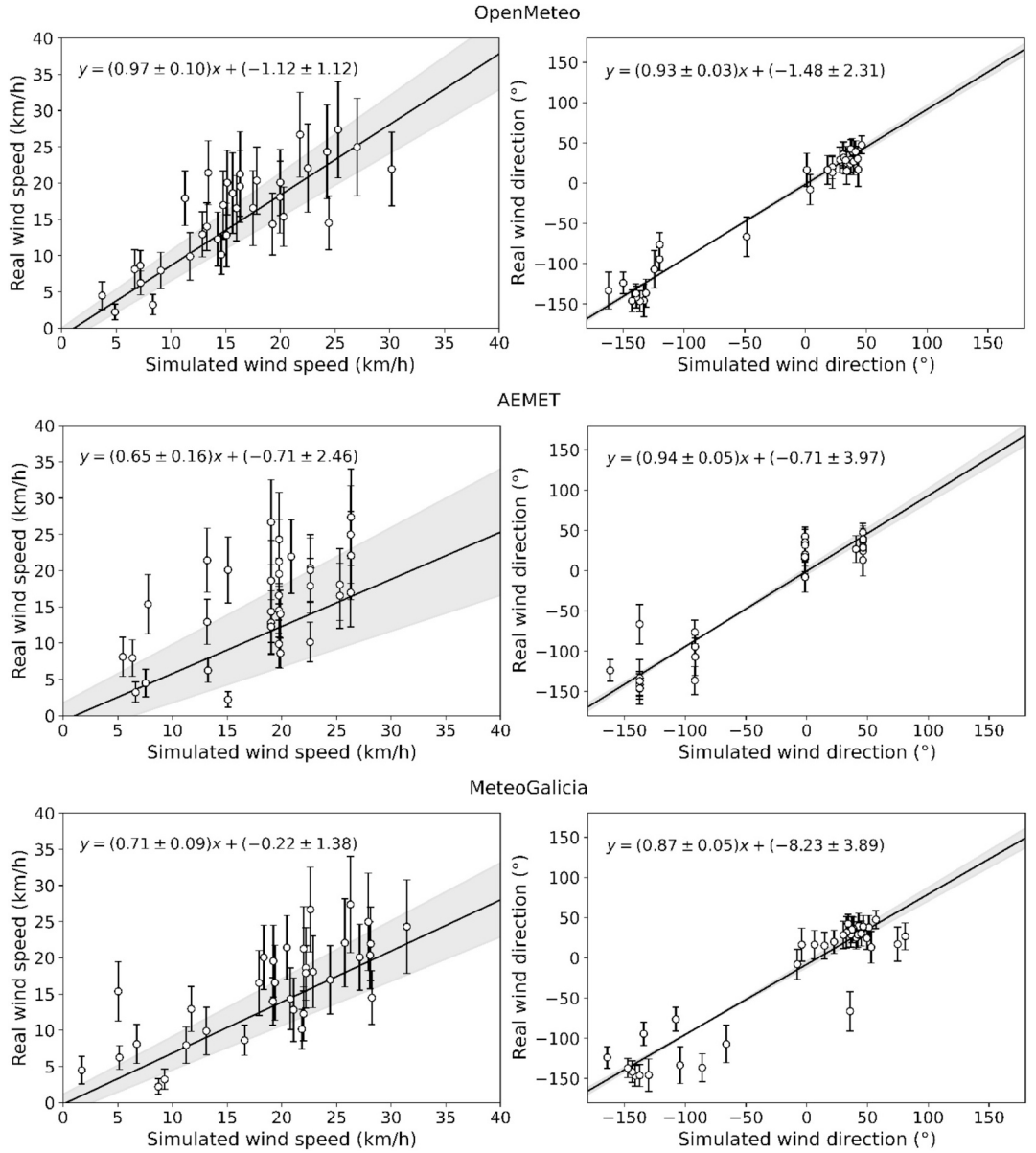

Fig. 7. Linear regression of the simulated and measured wind speeds (left column) and wind directions (right column) for the three weather services (OpenMeteo, AEMET, and MeteoGalicia). The gray area represents the highest and lowest possible straight lines using the parameter uncertainties of the linear fit, calculated as the square root of the diagonal components of the covariance matrix.

Table 1
CCC values for each prediction service.

	Wind speed	Wind direction
OpenMeteo	0.853	0.985
AEMET	0.627	0.959
MeteoGalicia	0.726	0.934

plus the transient wind tunnel simulation was done in less than two hours (around 10 minutes for the city reconstruction and one hour and a half for the wind tunnel), while all the execution and configuration of the other approach took more than a day. We have to keep in mind

that performing the simulation in an arbitrary path or scenario for the larger domain would yield slower results, as we would have

to reconfigure the mesh and all the drone settings. On the other hand, the wind tunnel simulation is already configured except for the boundary conditions, immediately extracted using a Python program, so the execution could be even faster. However, this computational gain would be useless if the results of both simulations were not comparable. In Fig. 8 we can see a comparison between both methodologies.

As we can see, results from both simulations are nearly the same, mainly in the lateral and lift forces, where the difference between both methods is practically negligible. The drag force seems to be consistently greater for the whole city simulation, in which some of the oscillations during flight are intensified. This can be caused due to the intrinsic instability of transient simulations, in which the size of the mesh might cause some variations even with constant boundary conditions. We have to keep in mind the great difference in mesh resolution between both cases, as the extracted wind data for the wind tunnel has a coarser mesh. Although mesh independence tests were performed, slight differences are to be expected. Other factors, such as the number of inner iterations or time step can explain the slight differences between both methodologies.

Overall, we observed a good agreement between the methodologies, which allowed us to verify the correct behavior of the wind tunnel test, reducing the simulation times of the drone inside the city domain while maintaining very accurate results. Thus, the wind tunnel test can be used as a fast tool to evaluate the loads over the drone surface following any complex trajectory within a reconstructed city domain, immensely simplifying the simulation setup process.

We wanted to test our reconstruction methodology in a real-life application and optimize it to the maximum in order to get the fastest possible results. As we have discussed, both the validation process of the urban CFD simulation and the comparison between both drone-path scenarios yielded satisfactory results.

4. Summary and conclusions

This study assessed the accuracy of various meteorological prediction models in reconstructed urban environments simulated via CFD, using real-life measurements for validation. The methodology accounted for both buildings and other constructions and surrounding vegetation patches. By integrating high-resolution urban geometries with meteorological data, we improved the reliability of CFD simulations for practical applications. Our results showed that corrected meteorological predictions significantly enhanced accuracy, confirming the proposed model effectiveness in forecasting wind speeds and directions in complex urban settings. A linear fit analysis revealed a strong correlation between OpenMeteo data and ground truth measurements, underscoring the robustness of our geometry reconstruction and boundary condition methods. Notably, the model also demonstrated solid performance even with lower-resolution input data.

Conversely, future forecasts from MeteoGalicia and AEMET—both of which are not updated beyond their initial 0:00 AM prediction—exhibited higher error margins. Nonetheless, these models still provided reasonable estimations of wind direction and speed, although they tended to slightly overestimate wind intensity. Interestingly, this overestimation can be advantageous in urban airflow simulations by ensuring conservative, worst-case scenario modeling, which is often desirable in safety-critical applications.

As commented in the introduction, the proposed methodology has broad applicability across fields such as urban planning, environmental monitoring, and UAV operations. Validation against ground-truth meteorological station data supports the credibility of the simulations and enhances confidence in their deployment for real-world decision-making. With the increasing global availability of LiDAR data, this approach can be easily adapted to cities worldwide, contributing to more informed urban management and planning strategies.

An important advantage of our framework is its high level of automation. Once the required datasets (LiDAR and cadastral data) are downloaded and a configuration file with basic spatial and temporal parameters is completed, the entire workflow—from geometry reconstruction to simulation and post-processing—is executed automatically, requiring no further user intervention. For small to medium-size simulations, results can be obtained in less than an hour, enabling rapid analysis of multiple scenarios and reducing the potential for errors associated with manual geometry creation.

We also applied this automated methodology to a moving drone scenario to simulate aerodynamic forces acting on the drone as it traversed the generated velocity field. We compared two modeling strategies: embedding the drone within the urban CFD simulation and using a wind tunnel-style test. The wind tunnel approach delivered comparable results but with significantly faster computational times, underscoring the practical benefits of our framework.

Although public LiDAR data is not yet available for all countries, broader availability is expected in the near future, which would facilitate wider adoption of the methodology. In addition, while RANS-based CFD simulations provide fast results, higher-fidelity approaches such as LES could improve accuracy in turbulent flow regions, requiring a balance between computational cost and precision. The inherent variability of real-world wind conditions, including gusts and rapid fluctuations, can also affect the accuracy of predictions. As a potential direction for future work, variable wind conditions could be introduced around the simulated flow fields to study optimal flight paths for drones under more realistic, fluctuating conditions.

In summary, this research presents a robust, adaptable methodology for integrating CFD simulations with meteorological predictions in urban environments. It proves effective in accurately reconstructing airflow patterns, allows rapid automated analysis with minimal user intervention, and provides practical utility for a wide range of real-world applications. The ability to quickly generate reliable wind fields and simulate their impact on dynamic elements such as UAVs marks a significant advancement in urban environmental modeling.

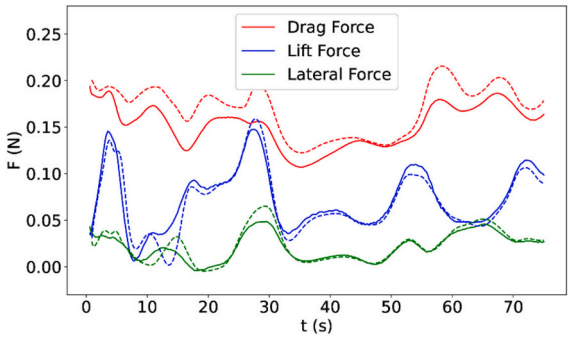

Fig. 8. Comparison of the forces acting over the drone geometry using both approaches. The dotted lines represent the results from the city reconstruction, while the full lines represent the wind tunnel test.

Acknowledgements

Some simulations were run using the Supercomputer Center of Galicia (CESGA) and we acknowledge their support. M. Suárez-Vázquez thanks the support of the Doutoramento Industrial program from GAIN-Xunta de Galicia (IN606D).

CRediT authorship contribution statement

Marcos Suárez-Vázquez: Writing – original draft, Visualization, Software, Methodology, Investigation, Formal analysis, Conceptualization. **Sylvana Varela Ballesta:** Writing – review & editing, Supervision, Resources, Methodology, Investigation, Conceptualization. **Alberto Otero-Cacho:** Writing – review & editing, Validation, Supervision, Resources, Methodology, Funding acquisition, Conceptualization. **Alberto P. Muñuzuri:** Writing – review & editing, Validation, Supervision, Resources, Methodology, Funding acquisition, Conceptualization. **Jorge Mira:** Writing – review & editing, Validation, Supervision, Resources, Project administration, Methodology, Funding acquisition, Conceptualization.

Declaration of competing interest

All authors declare that they have no conflicts of interest.

Appendix A. Supplementary data

Supplementary data to this article can be found online at https://doi.org/10.1016/j.uclim.2025.102664.

Data availability

Data will be made available on request.

References

Aliabadi, A.A., Veriotes, N., Pedro, G., 2018. A very large-Eddy simulation (VLES) model for the investigation of the neutral atmospheric boundary layer. J. Wind Eng. Ind. Aerodyn. 183, 152–171.
Allegrini, J., Dorer, V., Carmeliet, J., 2015. Coupled CFD, radiation and building energy model for studying heat fluxes in an urban environment with generic building configurations. Sustain. Cities Soc. 19, 385–394.
Alonso, M., Malpica, J., 2010. Satellite imagery classification with LiDAR data. Trees A 2106, 11.
Amukele, T., Ness, P.M., Tobian, A.A., Boyd, J., Street, J., 2017. Drone transportation of blood products. Transfusion (Paris) 57, 582–588.
Angel, S., Sheppard, S., Civco, D.L., Buckley, R., Chabaeva, A., Gitlin, L., Kraley, A., Parent, J., Perlin, M., others, 2005. The Dynamics of Global Urban Expansion. World Bank, Transport and Urban Development Department, Washington, DC.
Antoniou, N., Montazeri, H., Neophytou, M., Blocken, B., 2019. CFD simulation of urban microclimate: validation using high-resolution field measurements. Sci. Total Environ. 695, 133743.
Ayranci, Z.B., 2016. Use of drones in sports broadcasting. Ent Sports Law 33, 79.
Benarbia, T., Kyamakya, K., 2021. A literature review of drone-based package delivery logistics systems and their implementation feasibility. Sustainability 14, 360.
Biljecki, F., Ledoux, H., Stoter, J., 2016. An improved LOD specification for 3D building models. Comput. Environ. Urban. Syst. 59, 25–37.
Blocken, B., 2015. Computational fluid dynamics for urban physics: importance, scales, possibilities, limitations and ten tips and tricks towards accurate and reliable simulations. Build. Environ. 91, 219–245.
Blocken, B., Stathopoulos, T., Carmeliet, J., 2007. CFD simulation of the atmospheric boundary layer: wall function problems. Atmos. Environ. 41, 238–252.
Blocken, B., Janssen, W., van Hooff, T., 2012. CFD simulation for pedestrian wind comfort and wind safety in urban areas: general decision framework and case study for the Eindhoven University campus. Environ. Model Softw. 30, 15–34.

Bocquier, P., 2005. World urbanization prospects: an alternative to the UN model of projection compatible with the mobility transition theory. Demogr. Res. 12, 197–236.
Brozovsky, J., Simonsen, A., Gaitani, N., 2021. Validation of a CFD model for the evaluation of urban microclimate at high latitudes: a case study in Trondheim, Norway. Build. Environ. 205, 108175.
Chabot, D., Francis, C.M., 2016. Computer-automated bird detection and counts in high-resolution aerial images: a review. J. Field Ornithol. 87, 343–359.
Chu, A., Kwok, R.C.-W., Yu, K., 2005. Study of pollution dispersion in urban areas using computational fluid dynamics (CFD) and geographic information system (GIS). Environ. Model Softw. 20, 273–277.
de Miguel Molina, B., Segarra Oña, M., 2018. The drone sector in Europe. Ethics Civ. Drones Eur. Policies Propos. Ind. 7–33.
Dhunny, A., Samkhaniani, N., Lollchund, M., Rughooputh, S., 2018. Investigation of multi-level wind flow characteristics and pedestrian comfort in a tropical city. Urban Clim. 24, 185–204.
Di Nicola, F., Brattich, E., Di Sabatino, S., 2022. A new approach for roughness representation within urban dispersion models. Atmos. Environ. 283, 119181.
Eberly, D., 2008. Triangulation by ear clipping. Geom. Tools 2002–2005.
Fernández-Pacheco, V.M., Álvarez-Álvarez, E., Blanco-Marigorta, E., Ackermann, T., 2023. CFD model to study PM 10 dispersion in large-scale open spaces. Sci. Rep. 13, 5966.
Ferziger, J.H., Perić, M., Street, R.L., 2019. Computational Methods for Fluid Dynamics. Springer.
Fu, R., Padjen, I., García-Sánchez, C., 2024. Should we care about the level of detail in trees when running urban microscale simulations? Sustain. Cities Soc. 101, 105143.
Haidari, L.A., Brown, S.T., Ferguson, M., Bancroft, E., Spiker, M., Wilcox, A., Ambikapathi, R., Sampath, V., Connor, D.L., Lee, B.Y., 2016. The economic and operational value of using drones to transport vaccines. Vaccine 34, 4062–4067.
Hassan, G.E., Hassan, A., Youssef, M.E., 2014. Numerical investigation of medium range re number aerodynamics characteristics for NACA0018 airfoil. CFD Lett. 6, 175–187.
Ju, P., Li, M., Wang, J., 2021. Review of research advances in CFD techniques for the simulation of urban wind environments. Fluid Dyn. Mater. Process. 18, 449–462.
Koger, B., Deshpande, A., Kerby, J.T., Graving, J.M., Costelloe, B.R., Couzin, I.D., 2023. Quantifying the movement, behaviour and environmental context of group-living animals using drones and computer vision. J. Anim. Ecol. 92, 1357–1371.
Kundu, P.K., Cohen, I.M., Dowling, D.R., Capecelatro, J., 2024. Fluid Mechanics. Elsevier.
Li, M., Qiu, X., Shen, J., Xu, J., Feng, B., He, Y., Shi, G., Zhu, X., 2019. CFD simulation of the wind field in Jinjiang City using a building data generalization method. Atmosphere 10, 326.
Liu, S., Pan, W., Zhang, H., Cheng, X., Long, Z., Chen, Q., 2017. CFD simulations of wind distribution in an urban community with a full-scale geometrical model. Build. Environ. 117, 11–23.
Liu, S., Pan, W., Zhao, X., Zhang, H., Cheng, X., Long, Z., Chen, Q., 2018. Influence of surrounding buildings on wind flow around a building predicted by CFD simulations. Build. Environ. 140, 1–10.
Mirzaei, P.A., 2021. CFD modeling of micro and urban climates: problems to be solved in the new decade. Sustain. Cities Soc. 69, 102839.
Mishra, B., Garg, D., Narang, P., Mishra, V., 2020. Drone-surveillance for search and rescue in natural disaster. Comput. Commun. 156, 1–10.
Muñuzuri, A.P., Otero-Cacho, A., Mira, J., 2022. Ventilation time recommendation system incorporating local meteorological data. Indoor Built Environ. 31, 1418–1437.
Paden, I., García-Sánchez, C., Ledoux, H., 2022. Towards automatic reconstruction of 3D city models tailored for urban flow simulations. Front. Built Environ. 8, 899332.
Paden, I., Peters, R., García-Sánchez, C., Ledoux, H., 2024. Automatic high-detailed building reconstruction workflow for urban microscale simulations. Build. Environ. 265, 111978. https://doi.org/10.1016/j.buildenv.2024.111978.
Parente, A., Gorlé, C., Van Beeck, J., Benocci, C., 2011a. Improved k–ε model and wall function formulation for the RANS simulation of ABL flows. J. Wind Eng. Ind. Aerodyn. 99, 267–278.
Parente, A., Gorlé, C., van Beeck, J., Benocci, C., 2011b. A comprehensive modelling approach for the neutral atmospheric boundary layer: consistent inflow conditions, wall function and turbulence model. Bound.-Layer Meteorol. 140, 411–428.
Paz, C., Suárez, E., Gil, C., Baker, C., 2020. CFD analysis of the aerodynamic effects on the stability of the flight of a quadcopter UAV in the proximity of walls and ground. J. Wind Eng. Ind. Aerodyn. 206, 104378. https://doi.org/10.1016/j.jweia.2020.104378.
Paz, C., Suárez, E., Gil, C., Vence, J., 2021. Assessment of the methodology for the CFD simulation of the flight of a quadcopter UAV. J. Wind Eng. Ind. Aerodyn. 218, 104776. https://doi.org/10.1016/j.jweia.2021.104776.
PrabhakaraRao, P., Sampath, V., 2014. CFD analysis on airfoil at high angles of attack. Int. J. Eng. Res. 3, 430–434.
Pulver, A., Wei, R., Mann, C., 2016. Locating AED enabled medical drones to enhance cardiac arrest response times. Prehosp. Emerg. Care 20, 378–389.
Rajabi, M.S., Beigi, P., Aghakhani, S., 2023. Drone delivery systems and energy management: a review and future trends. Handb. Smart Energy Syst. 1–19.
Restas, A., 2015. Drone applications for supporting disaster management. World J. Eng. Technol. 3, 316–321.
Ricci, A., Kalkman, I., Blocken, B., Burlando, M., Freda, A., Repetto, M., 2017. Local-scale forcing effects on wind flows in an urban environment: impact of geometrical simplifications. J. Wind Eng. Ind. Aerodyn. 170, 238–255.
Rodi, W., 1991. Experience with two-layer models combining the k-epsilon model with a one-equation model near the wall. In: 29th Aerospace Sciences Meeting, p. 216.
Sandu, I., van Niekerk, A., Shepherd, T.G., Vosper, S.B., Zadra, A., Bacmeister, J., Beljaars, A., Brown, A.R., Dörnbrack, A., McFarlane, N., others, 2019. Impacts of orography on large-scale atmospheric circulation. Npj Clim. Atmos. Sci. 2, 10.
Shurupov, N., Molinero-Parejo, R., Rodríguez-Espinosa, V.M., Aguilera-Benavente, F., others, 2023. Clasificador Catastral: complemento de QGIS para la clasificación de los usos del suelo urbano a nivel de parcela. Bol. Asoc, Geógrafos Esp.
Siemens Digital Industries, 2024. Simcenter STAR-CCM+ user guide, version 17.02.007. In: Overset Mesh. Siemens, pp. 3158–3240.
Siemens Digital Industries Software, 2021. Simcenter \uppercaseSTAR-CCM+ User Guide v. 2021.1.
Toparlar, Y., Blocken, B., Maiheu, B., van Heijst, G.J.F., 2017. A review on the CFD analysis of urban microclimate. Renew. Sust. Energ. Rev. 80, 1613–1640.
Toparlar, Y., Blocken, B., Maiheu, B., Van Heijst, G., 2018. The effect of an urban park on the microclimate in its vicinity: a case study for Antwerp, Belgium. Int. J. Climatol. 38, e303–e322.
Valger, S., Fedorova, N., 2019. CFD methods in architecture and city planning. In: Journal of Physics: Conference Series. IOP Publishing, p. 012124.
Wang, X., McNamara, K.F., 2006. Evaluation of CFD simulation using RANS turbulence models for building effects on pollutant dispersion. Environ. Fluid Mech. 6, 181–202.
Wieringa, J., 1992. Updating the Davenport roughness classification. J. Wind Eng. Ind. Aerodyn. 41, 357–368.
Yang, L., Ye, M., others, 2014. CFD simulation research on residential indoor air quality. Sci. Total Environ. 472, 1137–1144.